# Joint Spatio -Temporal Registration of Retinal Angiograms

Shuoying Cao [1] Anil A. Bharath [1]
Kim Parker [1] Jeffrey Ng [1] John Arnold [2]
Alison H. McGregor [2] Adam Hill [2]
shuoying.cao@imperial.ac.uk

[1] Bioengineering Department
Imperial College London
[2] Imperial College Healthcare NHS Trust

**Abstract**

This paper addresses a 2D+t registration problem in retinal vascular analysis with specific application to the detection of microemboli. We propose a novel multi-stage Global-RANSAC registration model to perform intra- and inter-sequence spatial registration. First, a projective RANSAC algorithm is employed using a quadratic pairwise homography. This is applied in a local-then-global hierarchical 'joint' registration framework. Post-registration, vessel centrelines segmented by a scale space approach are used to construct a 'map' for comparing and monitoring temporal circulatory changes.

## Introduction

The accessibility of the retinal vascular system has spawned a huge range of clinical and pre-clinical research and diagnostic techniques as it provides a unique access point to the *in vivo* study of a complete vascular bed in a minimally invasive manner. Fluorescein angiography is a well-established technique for clinical access to the retina [1]. The passage of fluorescein dye through the retinal vessels reveals both the vessel structure and the rate of retinal blood flow. Measurements have linked changes in the human retinal vasculature with diseases such as hypertension, diabetes and age-related macular degeneration [2]-[4]. Leakage is associated with the breakdown of the blood–retina barrier; occluded vessels give rise to areas of impaired perfusion; microaneurysms or neovascularisation is indicated by the genesis of anomalous vessels [5]. These visible abnormal structural changes indicate the presence of later-stage diseases. However, for early-stage detection, the focus should be on capturing subtle changes in the retinal circulation. This requires establishing correspondence between microvasculature measures and retinal blood flow, and subsequent monitoring of one or more parameters over the course of time. Previously suggested parameters include blood flow velocity [6]; arteriovenous passage time [7]; difference of arterial and venous times to maximum intensity [8]; time to maximum image [9]. However, the high resolution imaging necessary to capture microvascular structures individually also needs registration of equivalent precision to accurately measure changes over time.

**Clinical Significance** In this paper, we take a fresh approach to detect subtle microvasculature occlusion, in the context of (micro)embolic surges during trauma or surgery, that could be associated with cognitive impairment or even morbidity [10]. Microemboli may cause reduced blood perfusion or even the apparent disappearance of vessels and/or vessel branches (microvascular occlusions). The occurrence of emboli is usually assessed clinically using Transcranial Doppler ultrasound (TCD) [11], but many emboli are smaller than the detectability threshold of TCD. Blauth *et al*. [4] therefore suggest that comparison of

© 2010. The copyright of this document resides with its authors.
It may be distributed unchanged freely in print or electronic forms.

pre- and post- operative retinal fluorescein images might indicate with greater sensitivity the existence of microemboli and provide a visual indication of the site(s) of occlusion. This is technically demanding as it requires access to information both at the pixel level and at the vascular structure level to establish the patient's vasculature 'map' both in pre- and post-intervention images, and is often complicated by temporal dynamics of blood flow. We therefore have two technical problems to solve: image registration and vessel segmentation. We need to geometrically align our sequences of angiograms into a common coordinate system (the reference), then to distinguish vascular segments from the background in the acquired images.

**Previous Relevant Work** Vascular bifurcation points labelled with vessel orientations, probability weighted by an angle-based invariant, were sorted according to respective likelihoods of assumed global affine transformation between frames by Zana *et al*. [12] using a Bayesian–Hough transform. Chanwimaluang *et al*. [13] extracted the medial axes of vessels as features. The similarity matrix for correspondence based on the centreline orientations was then converted to a prior probability that the extracted landmark locations were correct. Hierarchical estimation of the transformation model was performed, refining upwards from zeroth (translation), to first (affine), and finally the second (quadratic) order. Both of these approaches could be easily handicapped by inaccurate feature detection, resulting in false transformation estimation with a non-negligible *a posteriori* probability. Stewart *et al*. [14] put forward the dual-bootstrap iterative closest point (DB-ICP) algorithm. Small bootstrap regions are generated from hypothesized landmark correspondences and their surrounding vasculature, then progressively iterated upon to refine the transformation estimate. This approach requires accurate initialization of matching point correspondence.

# Methods

**Pairwise Registration** Arbitrary between-image distortion or degradation may arise due to geometric distortion, radiometric degradation, corruption by additive noise, and other changes in the scans to be described below. It is necessary to distinguish between image deformation (geometric 'noise') and the real change of the scene ('signal'). Furthermore, during clinical photography, the patient's head and eye can move relative to the camera during image capture. Many existing registration techniques do not deal with large geometric distortion other than perspective distortion (computer vision) and relative weak field distortion (MR imaging). Distortion in retinal scans was tackled by introducing spherical models [15]. While the retinal surface may be crudely approximated by a sphere, departures from this assumption induce some degree of error. This is further complicated by pixel intensity shifts due to the temporal diffusion of injected fluorescein dye confounded with uneven and unsteady global illumination.

At the pairwise level (registration applied to each pair of images in the set), we combine a projective RANSAC (iterative outlier rejection scheme) algorithm with a quadratic "pairwise" homography transformation, Figure 1(a). To ensure robustness and reliability regardless of geometric rotation and scaling, the bifurcation points or vessel crossings of a vascular tree (blood vessels) are generically regarded as a good source of landmark points (features). The Harris corner detector [16] enhanced by adaptive histogram equalization is relatively robust in feature extraction even when fluorescein dye concentration is rather low, commonly in the beginning (arterial phase) and the end (late venous and recirculation phase) of the angiogram sequence [1]. We putatively match these 'corners' by maximizing the normalized cross-correlation between the features from the sensed frame (the image that requires registration) with those from the reference frame, within windows surrounding each feature.

This comparison process filters out implausible correspondence pairs. The quadratic transformation model, with 12 degrees of freedom (see Equation 1), counteracts warping and is sufficiently flexible to reflect the spherical distortion introduced by retinal imaging geometry. Model parameter estimation benefits from both '*false* corner' rejection, near and beyond the image field-stops (see Section on Joint Registration), and [17]. RANSAC iteratively detects and rejects gross errors due to inaccurate local feature characterisation. Combined with a quadratic homography, the algorithm yields a high degree of accuracy even when a significant proportion of 'outliers' is present in the data set. Figure 1(b) & (c) compare between-frame pixel intensity differences without and with our pairwise registration model.

Let $\mathbf{p} = \begin{pmatrix} p_x \\ p_y \end{pmatrix}$, $\mathbf{q} = \begin{pmatrix} q_x \\ q_y \end{pmatrix}$ denote the feature-point coordinates from images P and Q, while $\mathbf{M} = \begin{pmatrix} m_0 & m_1 & m_2 & m_3 & m_4 & m_5 \\ m_6 & m_7 & m_8 & m_9 & m_{10} & m_{11} \end{pmatrix}$ denotes transformation model parameters, for $\mathbf{x}(\mathbf{q}) = (q_x, q_y, 1, q_x^2, q_y^2, q_x, q_y)^T$, the transformation can be represented as: $\mathbf{p} = \mathbf{M}\mathbf{x}(\mathbf{q})$ (1)

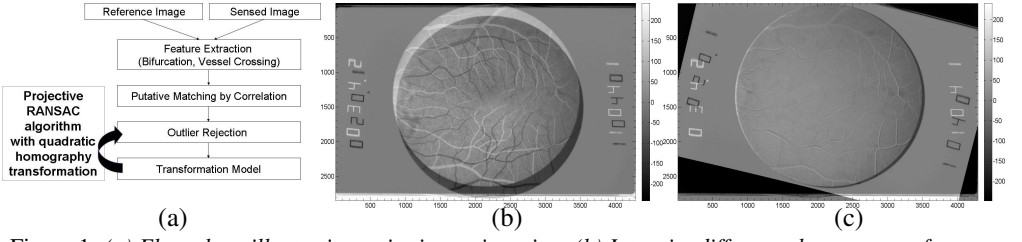


Figure 1: *(a) Flow chart illustrating pairwise registration; (b) Intensity difference between two frames half a sequence apart without pairwise registration (SD = 32.48); (c) Intensity difference between the two frames after pairwise registration (SD = 19.54).*

**Joint Registration** To compound temporal information both within a consecutive sequence of retinal angiograms (intra-sequence) and across sequences taken before and after the operation, separated by at least a few hours (inter-sequence), we need a systematic framework. This should first align corresponding pixels intra-sequentially, then align the pixels inter-sequentially. Multi-temporal registration is demanding as it is vital to maximize the point correspondence between similar structural features while still being able to differentiate or detect pathological changes of clinical interest. Temporal diffusion of injected dye and natural variability of blood vessels further complicate the *2D+t* joint-level registration problem. The centreline locations of the segmented vessels [18] have subpixel resolution and are less resilient to noise from misclassification. In clinical practice, capillaries may 'appear' then 'disappear' from sequential frames due to changes in dye concentration or acquisition noise. Images at the start and the end of the angiogram sequences reveal significantly less information about vascular structure than images obtained during the peak of dye concentration. We thus implement a scheme that takes into account centreline information at all times during the map construction. After initial segmentation of each frame, we impose a further constraint on the calculated centreline locations: for an extracted centreline to be valid, there must exist at least two frames in the sequence with similar location within a predefined city-block pixel distance. Each 'true' centreline location is stored to construct our compound maps.

Let us consider two time sequences of retinal data, acquired from unknown spatial locations, at unknown times relative to the cardiac cycle; we denote these unregistered time sequence images, by

$$\mathscr{S}^A = \left\{ f_n^A(x_n^A, y_n^A; t_n^A) \right\}_{n=1,2,3\ldots N_A} \text{ and } \mathscr{S}^B = \left\{ f_n^B(x_n^B, y_n^B; t_n^B) \right\}_{n=1,2,3\ldots N_B} \quad (2)$$

The goal of our registration task is to spatially register the intra-sequence images of $\mathscr{S}^A$ to a reference spatial coordinate system for that sequence, and to align images of $\mathscr{S}^B$ with their own reference coordinate system. We then register the two reference coordinate systems for $\mathscr{S}_A$ and $\mathscr{S}_B$. Finally, vessel maps $v_\alpha(x_A, y_A)$ and $v_\beta(x_B, y_B)$ are created by accumulating information across time about vessel centrelines, while incorporating consistency checks for registration and segmentation. Comparisons can then be performed between the maps for vessel centrelines $v_\alpha(x_A, y_A)$ and $v_\beta(x_B, y_B)$ to identify potential sites of vessel occlusion.

During the passage of the bolus of fluorescein, there will be a frame which contains a maximum in dye contrast. However, this does not justify it as the optimal choice of global reference. Instead, we construct a global reference frame for any sequence $\mathscr{S}_A$ as

$$f^A_{GR}(x^A_{GR}, y^A_{GR}; t^A_{GR}) = \arg\min_{n \in \mathscr{N}_A} \left\langle f^A_n(x^A_n, y^A_n; t^A_n) \times M^A_n(x^A_n, y^A_n; t^A_n) \right\rangle \tag{3}$$

where $\langle \cdot \rangle$ denotes a spatial average, and $M^A_n(x^A_n, y^A_n; t^A_n)$ is an appropriate spatial weighting function. We use a simple 2D mask containing unity for points $(x^A_n, y^A_n)$ within the circular region defined by the field-stop, and 0 outside this region. Other (*e.g.* centre) weighting functions could also be used. The centre and radius of this region are determined by a circular Hough Transform. Figure 2 illustrates this selection process. The peak in the plot (Figure 2(a)) of spatially averaged fluorescein concentration in the pre-op sequence against the frame number (corresponding to its acquisition time) determines the frame (highlighted in gray dashed-line in upper left quadrant in Figure 2(c)) as the global reference within the pre-op sequence. Meanwhile, Figure 2(b) illustrates the global reference of post-op sequence, framed by a dashed line in the lower right quadrant of Figure 2(c).

The global frame is not used immediately; rather, its location in time is used to establish a subdivision of the sequence $\mathscr{S}_\mathscr{A}$ into two sub-sequences $\mathscr{S}_{A1}$ and $\mathscr{S}_{A2}$. These subsequences are repeatedly subdivided until they are of length 3-5 frames. At this point, the mid-point of each sub-sequence is used as a *local* reference frame (e.g. $f^{A1}_{LR}(x^{A1}_{LR}, y^{A1}_{LR}; t^{A1}_{LR})$). Neighbouring frames are then spatially registered to these local reference frames. For example, for a sequence $\mathscr{S}_A$ of length 7 frames, two sub-sequences, $\mathscr{S}_{A1}$ and $\mathscr{S}_{A2}$, are obtained, with corresponding coordinate systems. These two local coordinate systems are co-registered to the global reference for $\mathscr{S}_A$. A similar process is applied to $\mathscr{S}_B$, separately. As a final stage, the two coordinate systems defined by $(x^A_{GR}, y^A_{GR}; t^A_{GR})$ and $(x^B_{GR}, y^B_{GR}; t^B_{GR})$ are registered.

Figure 2(c) exhibits a montage (from top-left to bottom-right, row-by-row) of both inter- and intra- sequentially aligned angiograms. A key feature is that the border of each frame in the pre-op sequence exhibits a visible rotation with respect to that of the post-op frames. In contrast, the centre of the fieldstop region from each frame seems nicely aligned with its neighbours. This demonstrates the success of this registration algorithm.

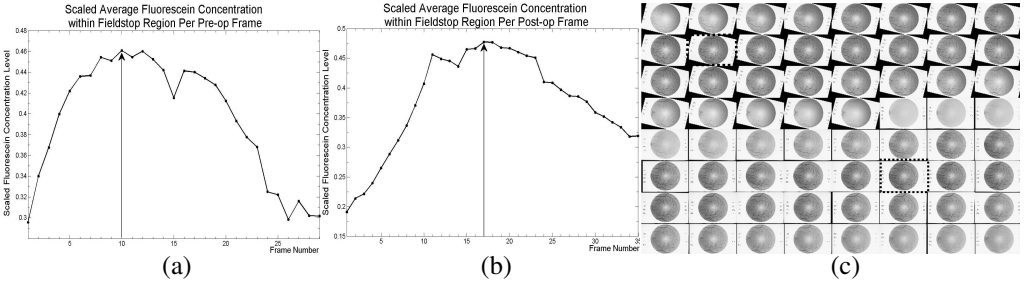


(a) (b) (c)

Figure 2: *(a) Pre-op spatially averaged fluorescein concentration against acquisition time; (b) Post-op spatially averaged fluorescein concentration against acquisition time; (c) Both global references in pre- and post- op sequences (framed by a dashed line) determined from the intensity-time course plots.*

# Conclusion and Further Work

Individual capillaries have been identified and quantified (see Figure 3) in fluorescein angiograms taken immediately pre- and post- orthopaedic surgery. The results compare well to non-quantitative conclusions of 'expert' observers who examined the original images.

Due to the difficulties of obtaining the ground truth for our retinal image analysis, we are hoping to validate our novel registration using a synthesized database, allowing us to justify our approach and to evaluate its accuracy and robustness. A known distortion, introduced manually, can be used to evaluate the registration components of the algorithm, while detecting a 'virtual' occlusion would validate our entire automation scheme.

Future development of this technique lies in extensive validation and real-time performance that could be adopted and evaluated in an inter-intervention setting. Notably, we are hoping to incorporate indicators of the success or failure of the registration process as a safeguard to prevent improper conclusions drawn on poorly registered images.

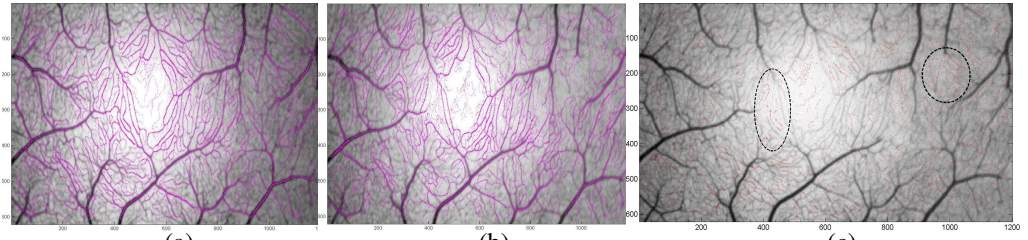

(a) (b) (c)

Figure 3: *(a) Macular vasculature centreline imposed on pre-operative fluorescein angiogram map; (b) Macular vasculature centreline imposed on post-operative fluorescein angiogram map; (c) Missing centreline pixels (in red) identifies sites (dashed circles) of microemboli.*

# Reference


1 H. R. Novotny, D. L. Alvis, "A method of photographing fluorescence in circulating blood in the human retina", Circulation.(1961), pp. 82-86.

2 A. V. Stanton, B. Wasan, A. Cerutti, S. Ford, R. Marsh, P. S. Sever, "Vascular network changes in the retina with age and hypertension", J. Hypertens. 13 (1995), pp. 1724-1728.

3 L. A. King, A. V. Stanton, P. S. Sever, S. Thom, A. D. Hughes, "Arteriolar length–diameter (L:D) ratio: A geometric parameter of the retinal vasculature diagnostic of hypertension," J. Hum. Hypertens. (1996), pp. 417-418.

4 C. Blauth, J. Arnold, E. M. Kohner, K. M. Taylor, "Retinal microembolism during cardiopulmonary bypass demonstrated by fluorescein angiography", Lancet 2 (1986), pp. 837-839.

5 G. Richard, "Fluorescein Angiography. Technique, Interpretation and Application" , Oxford University Press (1990)

6 O. Arend, S. Wolf, F. Jung, B. Bertram, H. Postgens, H. Toonen, M. Reim, "Retinal microcirculation in patients with diabetes mellitus: dynamic and morphological analysis of perifoveal capillary network", Br. J. Ophthalmol. 75 (1991), pp. 514–518

7 S. Wolf, F. Jung, H. Kiesewetter, N. Korber, M. Reim, "Video fluorescein angiography: method and clinical application", Graefe's Arch. Clin. Exp. Ophthalmol. 227 (1989), pp. 145–151

8 T. Koyama, N. Matsuo, K. Shimizu, M. Mihara, Y. Tsuchida, S. Wolf, M. Reim, "Retinal circulation times in quantificative fluorescein angiography", Graefe's Arch. Clin. Exp. Ophthalmol. 228 (1990), pp. 442–446.

9 J. H. Hipwell, A. Manivannan, P. Vieira, P.F. Sharp, J. V. Forrester, "Quantifying changes in retinal circulation: the generation of parametric images from fluorescein angiograms", Physiol. Meas. 19 (1998), pp. 165–180.

10 K. M. Taylor, "Brain damage during open-heart surgery ", Thorax 37(1982), pp. 873-876.

11 M. P. Spencer, G. I. Thomas, S. C. Nicholls, L. R. Sauvage, "Detection of middle cerebral artery emboli during carotid endarterectomy using transcranial Doppler ultrasonography", Stroke. 21(1990), pp. 415–423.

12 F. Zana, J. C. Klein, "A multimodal registration algorithm of eye fundus images using vessels detection and Hough transform", IEEE Transactions on Medical Imaging 18 (1999), pp. 419–428.

13 T. Chanwimaluang, G. Fan, S. R. Fransen, "Hybrid Retinal Image Registration", IEEE Transactions on Information Technology in Biomedicine 10(2006), pp. 129-142.

14 C. V. Stewart, C. L. Tsai, B. Roysam, “The Dual-Bootstrap Iterative Closest Point Algorithm with Application to Retinal Image Registration”, IEEE Transactions on Medical Imaging 22 (2003), pp. 1379-1394.

15 A. Can, C. V. Stewart, B. Roysam, H. L. Tanenbaum, “A featurebased, robust, hierarchical algorithm for registering pairs of images of the curved human retina”, IEEE Trans. Pattern Anal. Machine Intell., 24 (2002), pp. 347–364.

16 C. Harris, M. Stephens, "A combined corner and edge detector", Proceedings of the 4th Alvey Vision Conference (1988), pp 147-151.

17 M. A. Fischler, R. C. Bolles, "Random Sample Consensus: A Paradigm for Model Fitting with Applications to Image Analysis and Automated Cartography", Comm. Of the ACM. 24 (1981), pp. 381–395.

18 M. E. Martinez-Perez, A. D. Hughes, A. V. Stanton, S. A. Thom, A. A. Bharath, K. H. Parker, “Retinal blood vessel segmentation by means of scale-space analysis and region growing”, In: C. Taylor and A. Colchester, Editors, MICCAI-99, Lectures Notes in Computer Science vol. 1679, Springer-Verlag (1999), pp. 90–97.